Article

Holocene thinning in central Greenland controlled by the Northeast Greenland Ice Stream

Ilaria Tabone [1,2,3] ✉, Alexander Robinson [2,4], Marisa Montoya[2,5] &
Jorge Alvarez-Solas [2,5]

Ice-core records from the interior of the Greenland ice sheet suggest wide-spread thinning during the Holocene. However, the recurring underestimation of this thinning in numerical models raises concerns about both the veracity of such reconstructions and the reliability of glaciological models. Recent work suggests the 8000-year-old Northeast Greenland Ice Stream (NEGIS), including a now-extinct northern tributary, may have been an early influence on Greenland ice-sheet dynamics. Yet, the inaccurate reproduction of NEGIS-like dynamics in most models hampers investigation of whether this feature played a role in Holocene ice-sheet thinning. Here we show that grounding-line retreat in northeast Greenland triggers elevation changes at the northern summit via ice-dynamic effects modulated by the paleo NEGIS system. In our simulations, fast ice-stream flow caused by transiently imposed reduced basal shear stress following the northeast retreat explains 55% (± 18%) of the estimated ice thinning, showing that ice-stream dynamics is one of the main drivers of the NGRIP Holocene surface elevation drop. Our findings show that the ice-flow in northeast Greenland plays a large role in ice-surface elevation changes in central Greenland.

Understanding the history of the Greenland ice sheet (GrIS) during past warm periods is crucial to constrain its response to current and future climate change[1]. Local information retrieved from proxy records, such as the abrupt lowering of the ice surface elevation by several hundreds of metres (-200 to 1000 m) over the past 11,000 years estimated at ice-core sites[2,3], provides valuable insights into the local climate and/or ice-sheet evolution, as well as constraints for evaluating paleo ice-sheet models. Yet, the capability of correctly capturing this thinning represents a long-standing challenge for three-dimensional ice-sheet models[2–5]. Improved climate and isostatic rebound model representations have helped to reduce the early-Holocene (-11 ka ago) data-model mismatch at High Arctic, peripheral locations from 900 m to only 200 m[3]. Nevertheless, these features

cannot explain the reconstructed thinning at ice-core sites at lower latitudes, as High Arctic ice-elevation changes are mainly driven by the polar amplification, glaciostatic effects resulting from the demise of the nearby North American ice sheets[3], and changes in precipitation[2]. Thus, the reasons behind the prominent thinning in central Greenland, such as the ~200 m elevation drop estimated at the NGRIP site[2], remain unclear.

The proximity of the ~600 km-long Northeast Greenland Ice Stream (NEGIS, defined here as all ice stream branches and all outlet glaciers) to the ice divide at the present[6], as well as the presence of another well-defined NEGIS-like stream stretching north from the 79°N glacier far to the interior during the early Holocene[7], suggest a possible far-reaching influence of ice-stream dynamics during the Holocene

[1]Departamento de Geofísica, Universidad de Concepción, Concepción, Chile. [2]Departamento de Física de la Tierra y Astrofísica, Facultad de Ciencias Físicas, Universidad Complutense de Madrid, Madrid, Spain. [3]Institute of Geography, Friedrich-Alexander University of Erlangen-Nürnberg, Erlangen, Germany. [4]Alfred Wegener Institute, Helmholtz Centre for Polar and Marine Research, Potsdam, Germany. [5]Instituto de Geociencias, Consejo Superior de Investigaciones Científicas-Universidad Complutense de Madrid, Madrid, Spain. ✉e-mail: itabone@dgeo.udec.cl

(Fig. S1). Yet, large uncertainties in basal processes driving the NEGIS-like flow hamper its proper model representation[8]. The inclusion of subglacial hydrology schemes[9], as well as extremely high basal geothermal heat flow (GHF)[10], has improved the ability of models to simulate the present NEGIS fast flow. Surface-velocity assimilation for basal shear stress estimation yields the most accurate basal friction approximation, although only where the bed is currently temperate, assuming a specific temperature profile. Yet, assumptions of steady-state basal dynamics are only valid for decades-long simulations. The dynamics of the ice sheet can change considerably as the time scale increases due to non-negligible variations in the drainage system and changes in its geometry[7]. Therefore, the simulation of the paleo NEGIS flow pattern on multi-millennial time scales is a challenging task. Accordingly, its potential role in the GrIS evolution, in particular in the dramatic early Holocene thinning, remains unexplored.

Here, we investigate the impact of the NEGIS dynamics on the Holocene surface elevation drop in north-central Greenland. We perform an ensemble of 3000 simulations of the GrIS evolution through the last deglaciation using a state-of-the-art, three-dimensional, thermomechanically coupled ice-sheet model[11] specifically adapted to represent various configurations of the paleo NEGIS (see the "Methods" section for details). The accurate timing of the deglaciation is ensured by evaluating the model results against deglaciation timings inferred from marine sediment records from the Northeast Greenland continental shelf. We characterise the past northeast fast flow regime as a system of a northern, now-extinct paleo ice stream and a southern present-day-like ice stream that activated during the Holocene by imposing a time-dependent basal friction change beneath the NEGIS (Fig. S1). Such a stream configuration is in line with recent improvements in our understanding of this system[7]. Basal lubrication is promoted by reducing the bed-dependent basal friction coefficient and by imposing sufficiently high GHF[12], which results in high sliding rates for the ice-stream system during most of the Holocene. We find that

NGRIP thinning is initiated by the NEGIS onset, enhanced by upstream propagation following early Holocene ice-sheet retreat in northeast Greenland, and maintained by increased meltwater production and reduced basal friction. The far inland development of the present-like NEGIS during the last 8 kyr, here fostered by imposing a time-dependent reduced basal friction coefficient along the ice stream, drives the dynamic thinning, explaining at least ~100 m of the surface elevation drop in north-central Greenland. Such a far-inland reach of dynamic thinning in northeast Greenland during a major retreat phase suggests that such processes may also amplify the response of this sector to future warming and ice loss.

Results and discussion
The Northeast Greenland Holocene retreat

Our transient simulations show a progressive inland retreat of the northeastern sector throughout most of the Holocene (Figs. 1 and S2). At the end of the Last Glacial Maximum (LGM), the grounded ice sheet extends over the continental shelf, in agreement with reconstructions[13]. The ice-stream configuration at the onset of the deglaciation shows three well-defined fast-flowing regions draining ice mass from the present-day location of the Nioghalvfjerdsbrae (79°N) and Zachariae Isstrom (ZI) outlet glaciers to the shelf break. Two topographically constrained ice streams flow over the northern and southern troughs, whilst a third stream flows eastward over the shallow bank. The location of this ice-stream system aligns with glacial lineations mapped in the area from bathymetry data[13]. An ice stream flowing eastward and draining the shallow bank between the troughs would support the hypothesis of the GrIS extending toward the shelf edge during the LGM[14].

Deglaciation began ~15 kyr ago when a rapid annual air temperature rise drove ice-sheet retreat to today's ice front by about 10 kyr ago (Figs. 1 and 2). In our simulations, the NEGIS ice front retreats from the outer to the inner coast between 11.7 and 10.2 kyr ago, followed by
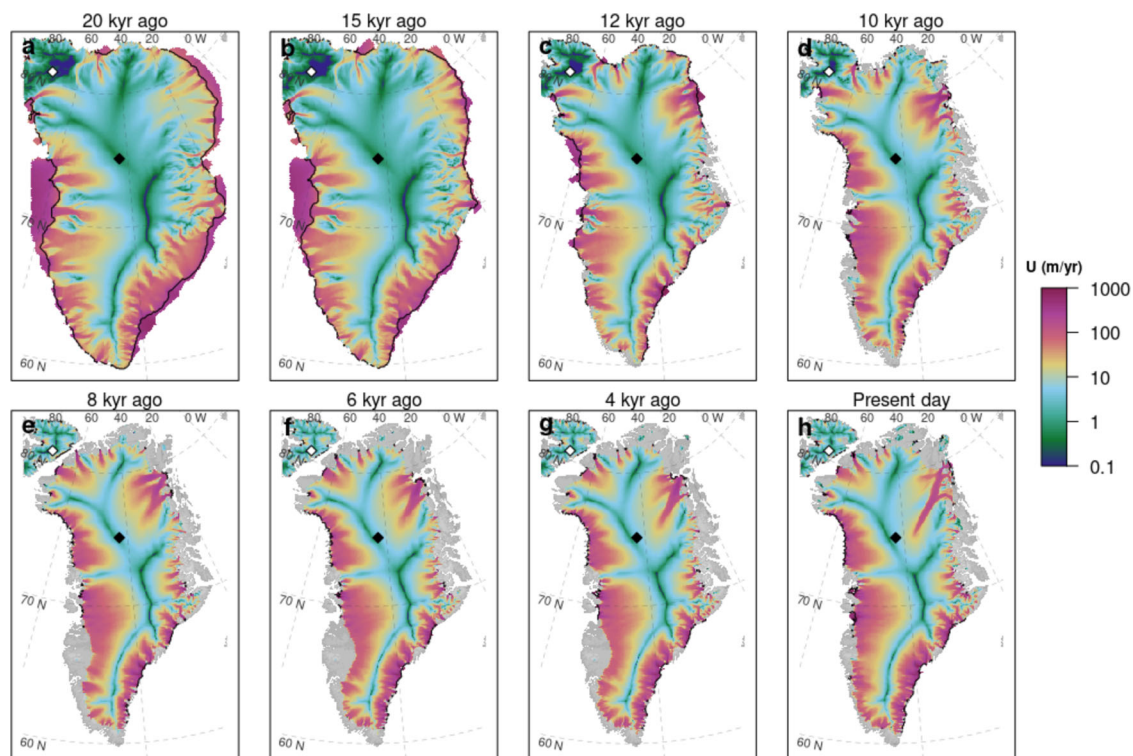

Fig. 1 | Greenland ice dynamics during the last deglaciation. Greenland ice surface velocity (m/yr) modelled in the ensemble best simulation (see Fig. 4) at different times from the Last Glacial Maximum (~20 kyr ago) to the present (panels from **a**–**h**). Black lines represent the grounding line, and velocities outside these represent ice shelf velocities. The black and white diamonds show the North Greenland Ice Core Project (NGRIP) and the Agassiz drilling sites, respectively.
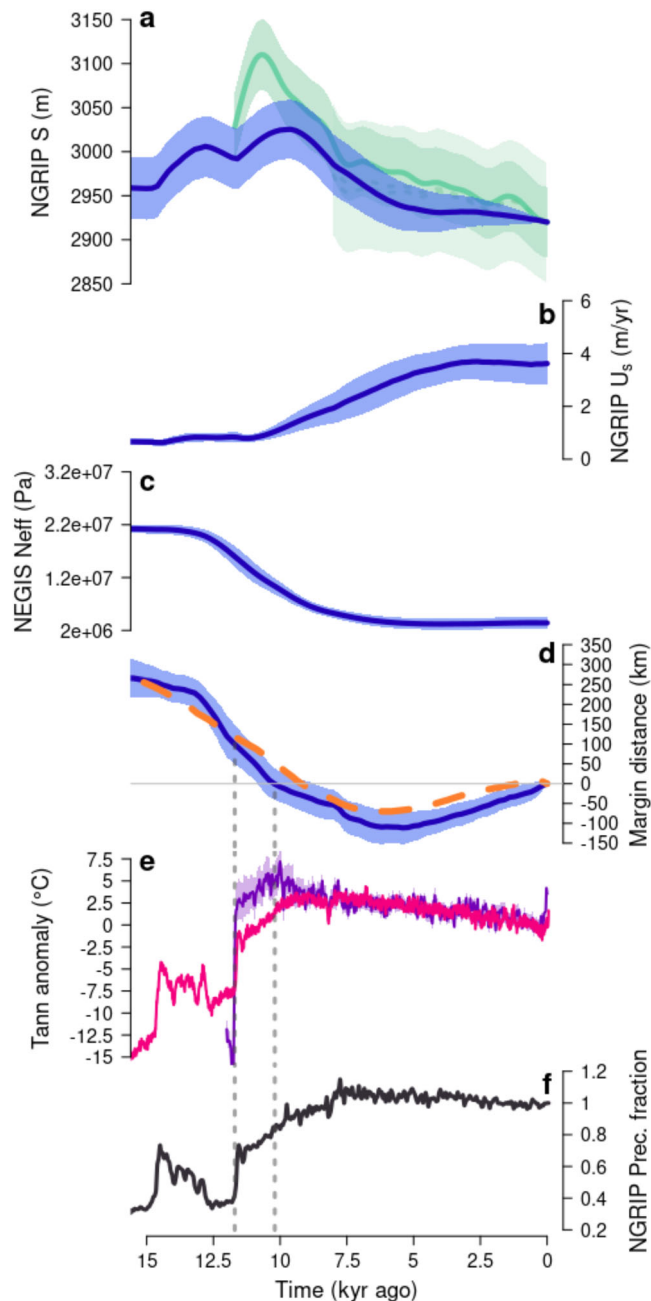
Fig. 2 | 15,000 years of Northern Greenland evolution and climate forcing.
Modelled (blue, this work) and reconstructed (green) surface elevation at the
North Greenland Ice Core Project (NGRIP) ice-core location (**a**); reconstructions
from[2] (~12–0 kyr ago) and[4] (8–0 kyr ago) are shown with their mean elevations
(thick and dashed green lines, respectively) and 1−σ uncertainties (darker and
lighter shaded green, respectively). Surface velocity modelled at NGRIP (**b**), and
simulated effective pressure averaged over the Northeast Greenland Ice Stream
(NEGIS) basin (**c**). Modelled distance of the ice front position from the present
position at 79°N glacier (see Fig. S1), one of the NEGIS outlet glaciers[6], with
reconstructed ice front evolution from[14] (orange dashed curve) (**d**). Annual air
temperature anomaly (**e**) reconstructed at 79°N from climate modelling
improved by δ^{15}N ice-core data (pink[24]); temperature reconstructed at Agassiz
from δ^{18}O and ice melt data is shown in purple (with 1−σ uncertainty shaded)[3].
Precipitation fraction at NGRIP (**f**) with respect to the present day retrieved from
paleoclimate data assimilation[25]. Grey dotted vertical lines show the retreat of
79°N from the outer to the inner shelf. Yelmo model ensemble results in **a–d** are
shown with their score-weighted mean (thick blue line) and 1−σ uncertainty range
(inner shaded blue).

a further recession of several tens of kilometres (~110 ± 40 km) 7–5 kyr
ago (Fig. 2d). Such a retreat history compares well with cosmogenic-
based Holocene ice-front reconstructions[14] (see Fig. 2d) and
independent ^{14}C-exposure dating of marine organic material[15].
Although the retreat at the present 79°N ice-shelf front is simulated
~1 kyr earlier than in data (Fig. 2d), the timing of the outer-to-inner shelf
recession aligns closely with deglaciation timings of both moraines at
today's NEGIS ice front[14,15] and marine locations in the northeast shelf
derived from gravity core analysis (blue dots and triangles of Fig. 3,
respectively).

The fast inland retreat simulated at the early Holocene is accom-
panied by the formation of a paleo-NEGIS stretching from the northern
flank of present-day NEGIS outlet glaciers into the ice-sheet interior
(Fig. 1). The catchment shows three main well-defined north-to-south
outlets and replaces the system of fast glaciers simulated over the
northeastern shelf during the LGM. Increased sliding velocities pro-
pagate upstream in response to thermo-mechanical and geometrical
changes occurring during the retreat of the marine-based ice sheet,
through an imposed basal friction coefficient reduction through time.
At the onset of the deglaciation, ice-mass loss at the shelf edge due to
rising air and oceanic temperatures (Fig. S3) weakens buttressing,
accelerating inland ice flow. This results in glacier thinning, ice flow
speed-up, and retreat of the grounding line, which further accelerates
the ice flow, promoting ice-front recession. Although ice thinning at
the front reduces basal friction (as effective pressure decreases),
sliding significantly increases when a local increase in subglacial melt
occurs due to increased frictional heating (Fig. S4). As the retreat
continues, regions showing decreased basal friction conditions allow
for flow acceleration farther upstream toward the ice divide (Fig. 2).

Our simulations first show a surface elevation increase in north-
central Greenland from 12 to 9.4 kyr ago (Fig. 2a), mostly due to
increased precipitation[2] (Fig. 2f). Then, the velocity propagation
associated with the imposed inland expansion of the paleo-NEGIS
induces dynamic thinning of ice at the NGRIP site (Fig. S5). Northern
summit ice is advected downstream, causing the surface elevation to
decrease abruptly (Fig. 2a) until the end of the Holocene Thermal
Maximum (HTM) (~5 kyr ago). For the last 5 kyr the northeastern ice
front slowly regrows towards its present position, reducing the NGRIP
surface ice velocity (Fig. 2b) and the rate of thinning (Fig. 2a). Yet, the
decrease in basal sliding imposed at the present NEGIS (Fig. S1) ensures
continuous drainage of the GrIS northern sector until the present
(Fig. 1). The hypothesis of the presence of a large, active ice stream
resembling that of today since the mid-Holocene is further supported
by a recent study of past ice-flow trajectories connecting the EGRIP ice
back to its source location[16].

Influence of ice stream dynamics on the NGRIP thinning
The surface-elevation increase induced by the rise in precipitation at
the early Holocene is rapidly followed by a significant drop persisting
until the late Holocene (Fig. 2a). We simulate a score-weighted mean
(see the "Methods" section) maximum elevation change of 105 ± 34 m,
corresponding to 55 ± 18% of the reconstructed 190 m surface-
elevation fall[2] (Fig. 4). Yet, the model scenario showing the highest
thinning within the score-weighted 1−σ uncertainty shows a maximum
elevation drop of 139 m, indicating that up to 73% of the total esti-
mated thinning is reproduced.

We propose that the mechanism behind the early-Holocene GrIS
north-central thinning is its dynamic adjustment to the NEGIS-induced
inland flow acceleration during margin retreat (i.e. the retreat of the ice
front and associated drainage basin). This hypothesis is in agreement
with studies from extinct ice streams in Canada and Iceland, suggest-
ing that the dynamic switch of paleo-ice streams has crucial
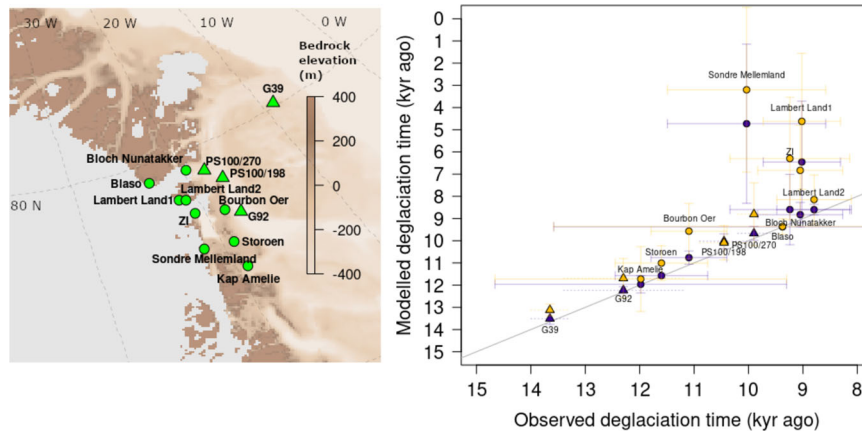consequences on ice-sheet stability[17,18]. To test this hypothesis, we

Fig. 3 | Northeastern air-temperature forcing controlling margin retreat. Inferred and modelled deglaciation times (right panel) for different locations in Northeast Greenland from the outer to the inner coast (left panel). Location of sediment cores (triangles[31–34]) and moraines (circles,[14]), from which the deglaciation timing has been reconstructed, are shown with triangles and circles, respectively

(left panel). Deglaciation times are modelled for two different Holocene air-temperature reconstructions (see Fig. S17, right panel[24] (blue line) and (yellow line)[25]. The 1:1 line in the right panel is shown in grey. Dotted and solid error bars represent uncertainties in deglaciation timings for sediment cores and moraines, respectively.
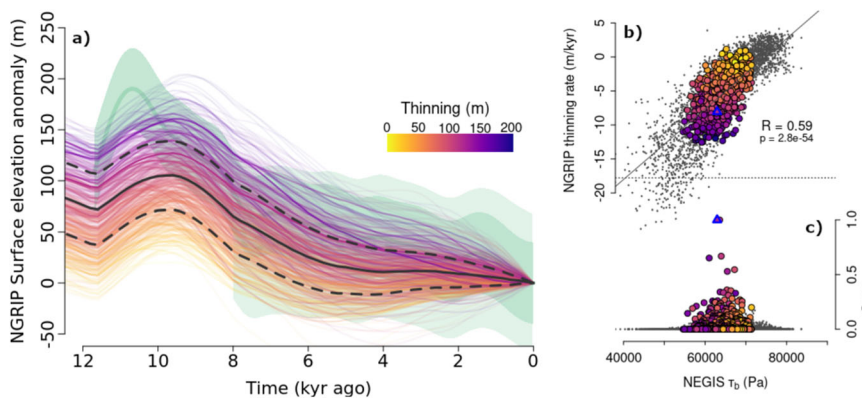

Fig. 4 | Thinning and ice-flow relationship in north-central Greenland. Last 12 kyr of surface elevation change for all ensemble members (**a**); valid simulations are shown by thin lines coloured according to the total amount of thinning across the Holocene at the North Greenland Ice Core Project (NGRIP) ice-core location (computed as the difference between the time of maximum elevation during the Holocene and the present) and are more transparent as their score diminishes; black thick and dashed black lines represent the score-weighted ensemble mean and 1−σ uncertainties, respectively; NGRIP elevation-change reconstructions are

shown in green as in Fig. 2a. NGRIP thinning rates (**b**) and final scores, where 1 represents the best simulation (**c**), for each model simulation as a function of the mean-Northeast Greenland Ice Stream (NEGIS) basal shear stress. Thinning rate and shear stress are averaged between the time of Holocene maximum elevation and the present; coloured points follow the colour palette of panel (**a**); discarded simulations are shown as grey dots; correlation coefficient and *p*-value for scored simulations are also reported. The best simulation of the ensemble is shown as a blue triangle.

investigate the relationship between the NEGIS dynamics, as defined by its basal sliding state, and the nearby NGRIP elevation change. We find that the NGRIP Holocene thinning rate is well correlated with the NEGIS basal shear stress ($R = 0.59$; Fig. 4b, c), calculated as the average between all the NEGIS catchments (northern, central and southern branches), with the strongest dependence for the early-mid Holocene interval with respect to the late Holocene (Fig. S6). This implies that faster sliding in the proximal NEGIS onset zone enhances thinning at NGRIP, which intensifies as the ice-stream onset propagates inland. No similar correlation is found for any other GrIS basins in our experiments (Fig. S7), indicating that there is no other catchment where ice flow plays a significant role in the NGRIP thinning.

The bed-elevation-dependent basal friction coefficient strongly controls the ice-stream basal conditions, hence the NGRIP thinning (Fig. S8). The imposed changes in the basal friction coefficient (Fig. S1) represent any transient processes at the base of the ice sheet not explicitly represented in the model. These could include changes to bed roughness due to sediment transport and deposition, as well as

changes in subglacial drainage and routing. Yet, basal lubrication from melting enhances the flow. In our simulations, the initial increase in velocity is associated with dynamic adjustment due to ice-margin retreat (Fig. S5), which causes a decline in the basal effective pressure and friction, and an increase in meltwater production stemming from increased frictional heating. Sustained basal melt rates at the early Holocene saturate the basal till within a few thousand years, promoting a progressive upstream decrease in basal traction and faster flow (Fig. S4). Here, a mean GHF of ~63 mW/m²[12] is required along the NEGIS flowline to reproduce the rapid NEGIS inland expansion upon ice-flow acceleration needed to drive a significant NGRIP elevation drop (Fig. S9). Despite even higher GHF values suggested in northeast Greenland as attributed to the passage of the Icelandic hotspot[19], a GHF of just 63 mW/m² allows our model to simulate a temperate bed at the NEGIS, in line with estimates[20]. The high basal melting rates modelled for the same region are also in agreement with recent work[21].

Model simulations with a very fast ice stream result in a larger Holocene NGRIP thinning (Fig. 4b, grey points). Yet, these tend to

present an overall low skill score (Fig. 4c), mainly due to mismatches in the simulated present NGRIP elevation, northeast geometry, and ice-ocean front position (Fig. S10). Here the NEGIS bed roughness parameter is set to a constant value for each experiment. The internal switch applied at the mid-Holocene (Fig. S1) and the time-dependent variables in the friction law (effective pressure, see Eq. (4) and scaling parameter λ depending on bedrock elevation, see Eq. (3)) introduce some time variability in the definition of the friction coefficient. However, these approximations, the coarse model resolution and the simple hydrology model employed here are otherwise insufficient to reproduce the complex, unsteady dynamic state of the ice stream due to continuous fluctuations in the basal water system[22]. The inclusion of physical processes important for describing present-day ice-stream behaviour, such as non-local basal water routing[9] could allow for a better investigation of the complex NEGIS dynamics in the future. Such complex behaviour of the NEGIS observed at present might still reflect the response to large geometry adjustments that occurred during the last deglaciation[22,23], likely associated with a substantial change in the streaming activity in northeast Greenland during the Holocene[7].

Early-Holocene temperature in the Northeast

We investigate the role of forcing climatology in the Holocene retreat by running an additional 3000-member ensemble experiment for a different deglaciation temperature scenario. This suggests a high sensitivity of the northeast margin retreat to the climate forcing (Fig. 3). The Holocene temperature anomaly based on ice-core-adjusted climate model simulations[24] is here replaced by independent paleoclimatic reanalysis reconstructions[25]. Both scenarios are based on the transient climate Trace-21ka experiment[26], yet the diverse ice-core data and techniques used to improve the original climate outputs may result in temperature differences, enhanced in areas with poor proxy records for model evaluation. This is clear at the NEGIS ice front, where significant discrepancies are present at the early Holocene (Fig. S17, right panel, yellow and blue lines). We find that temperature reconstructions that peak earlier (-9 kyr ago) and higher (+3.5 °C with respect to preindustrial levels) in the northeast sector are crucial for a correct retreat (Fig. 3).

A comparison of our two ensembles points to an early-Holocene temperature transition that should be closer to that estimated for the Agassiz ice cap[3] (Fig. S17, right panel). Yet, the latter shows an even sharper (+7 °C compared to pre-industrial levels) and earlier (10 kyr ago) glacial-interglacial temperature rise, which could be related to high-latitude amplification effects[24]. An early HTM (11–7 kyr ago) would also be supported by marine proxy records in the Northern Hemisphere[27]. Summer air temperatures at EGRIP in the early Holocene could have been 3 °C higher than today[28], while northwest and central Greenland could have been even warmer (3–5 °C)[29].

Interestingly, our early northeast retreat is in contrast with the ice-front recessional pattern found in southwest Greenland associated with a late HTM[30]. This heterogeneity in time and magnitude of warming trends may be interpreted as the climatic response to regional effects that are reflected in the asynchronous ice-front retreat.

Drivers of the northeast retreat

Simultaneous air and ocean temperature increases took place around -15 kyr ago (Fig. S3), but submarine melting only occurred 13.3 kyr ago when the oceanic temperature anomalies increased by 2 K from their glacial value (see the "Methods" section). Simulations with extremely low oceanic forcing ($\kappa \sim 0$) still simulate a retreat from the continental shelf, potentially causing rapid thinning at NGRIP (Fig. S8). This implies that in our model, initial deglaciation in the northeast is triggered by atmospheric warming. Elevated air temperatures intensify surface ablation, thin the floating tongues, accelerate ice flow, and lead to ice front retreat. Sensitivity tests using different climatologies highlight a primary control of atmospheric temperatures on inner shelf retreat timing (Fig. 3, e.g. Sondre Mellemland, Lambert Land).

Still, introducing a significant ocean temperature anomaly at -13 kyr ago (see the "Methods" section and Fig. S3) is crucial for accurately modelling the Holocene retreat rate. Initial tests with water temperature data from Trace-21 ka exhibited a consistent delay in the mid-inner shelf retreat (not shown). Abundant evidence from sediment core analysis supports the presence of Atlantic Waters (AW) on the outer continental shelf as early as -13.4 kyr ago[31,32] and on the inner shelf during the early Holocene (-11 kyr ago)[33,34]. This hints at the potentially significant role of warmer ocean temperatures in the disintegration of the northeast ice sheet's floating front and grounding-line migration during the last deglaciation.

The central role of the oceanic forcing in the northeast ice sheet's retreat could be similar to that observed at the present. Ice depletion at the grounding line of 79°N and ZI due to increased water temperature is the principal cause of their current retreat[35]. In the case of ZI, air temperature warming decades ago reduced sea ice, promoting calving and floating tongue collapse, decreasing buttressing on the glacier[36]. However, the present ZI grounding-line recession is predominantly attributed to the intrusion of warmer North AW in the fjord[35], an effect seen persisting until a topographic ridge stabilises the retreat[37]. Topography restrained AW inflows at the 79°N glacier front[38], yet recent observations reveal warmer waters beneath the ice shelf and near the grounding line[39], causing the ice tongue to lose most of its mass through submarine melting. The potential collapse of the floating tongue would have severe implications for the near-future stability of the glacier, as reduced buttressing prompts acceleration, thinning, and grounding-line retreat.

We propose that the northeast margin retreat occurred due to a combination of warmer air and oceanic temperatures. The abrupt air temperature increase (>15 °C) around -15 kyr ago initiated the retreat through enhanced surface ablation, thinning the ice front and favouring grounding line retreat. Warming AW on the northeast shelf since -13 kyr ago likely amplified the retreat through increased submarine melting at the grounding line, fostering ice margin instability and accelerating inland retreat. Sea-ice buttressing is not simulated here, therefore its potential impact cannot be evaluated.

Extended dynamic effect of the retreat on the interior of the ice sheet

The NGRIP lowering can be interpreted as the indirect response to margin retreat via geometry and subglacial water system alterations. In our simulations, the northeast ice sheet's retreat during the last deglaciation has an extended dynamic effect on the ice-sheet interior (Fig. S5). Margin thinning and retreat, driven by the early Holocene temperature rise, induce velocity propagation at higher elevations, causing ice thinning, reducing effective pressure and increasing basal sliding (Fig. S4). Still, basal sliding increases considerably only when a significant basal water increase from enhanced basal frictional heating saturates the till. This reduces the effective pressure and basal friction, increasing velocity along the ice stream and allowing upstream paleo-NEGIS propagation (Fig. S11). Notably, the onset of the NGRIP dynamic thinning (and surface elevation drop) occurs independently of whether basal friction beneath the NEGIS is artificially reduced or not, since it is triggered by the dynamic adjustment and velocity propagation in the northeast caused by margin retreat (Fig. S5). In fact, the NGRIP thickness decrease occurs following the decrease in basal friction at EGRIP, which in turn follows the decrease in basal drag averaged at the NEGIS basin due to margin retreat (Fig. S12).

Still, the imposed reduction in the basal friction enhances the dynamic thinning and velocity increase at higher elevations throughout the rest of the Holocene. This is primarily due to an earlier saturation in the hydrological system and a structural enhancement of inland velocity once saturation occurs. The extensive and sustained dynamic effects of the retreat, evident in the best simulation, contrast starkly with the limited impact observed in an unperturbed test

simulation where a constant $c_f = 1$ is imposed (Figs. S4, S11, and S13). Indeed, in this unperturbed simulation, the constrained velocity increase toward the ice divide limits the NGRIP dynamic thinning for the duration of the Holocene. Therefore, although the NGRIP thinning is triggered by the northeast retreat and the dynamic adjustment associated with it, independently from the applied NEGIS basal friction coefficient, the sustained thinning during the Holocene is controlled by the high sliding environment at the NEGIS, here favoured by the imposed reduced basal friction coefficient.

It has been shown that, over time spans ranging from centuries to millennia, variations in surface elevation trigger a corresponding reaction in the basal water drainage system (and vice versa)[22]. As a result, adjustments in thickness and velocity can extend several hundred kilometres inland through wave propagation[40]. Long-term ice-flow acceleration can be propagated at almost the highest elevations in the ice sheet as a result of mass loss at the terminus[41]. This has been observed at ZI recently, where the ice front retreat of -10 km has induced dynamic thinning along the NEGIS more than 200 km upstream[42]. This has also been observed in some glaciers in west Greenland[43]. Moreover, localised perturbations at the Antarctic ice-shelf front have been shown to propagate even more than 900 km upstream along the ice stream[44]. These findings align with our hypothesis that ice acceleration and ice front retreat in northeastern Greenland could have induced dynamic thinning more than 600 km from the ice front on centennial to millennial timescales.

Secondary effects on NGRIP thinning from other parameters

Ice anisotropy, controlled by ice temperature and stress variations, exerts a major control on the NGRIP dropdown during the Holocene (Fig. S8). Stiffer ice (represented via a lower value of E_{shear} in our model) in shear-controlled areas promotes slower ice flow, hampering upstream dynamic mass loss and facilitating the surface elevation increase at the early deglaciation. Although the enhancement factor varies spatially across the ice sheet (see the "Methods" section), we do not investigate how different streaming flow factors might affect the dynamics of fast flow. Still, our simulations show higher ice viscosity for ice stream regions ($E_{stream} = 1$, $E_{shear} > 1$, see the "Methods" section and Table S1). This agrees with flow factors recently estimated at the NEGIS from radar and ice-flow modelling, suggesting stiffer ice along the stream flow and softer at the shear margins[45]. Although simulations with slower ice flow show greater accuracy in predicting ice thickness within the northeast catchment, they simulate too much ice in the ice sheet interior at present (Fig. S10). This highlights the need for spatial variability in most parameters (e.g. c_f from Eq. (2) and f_p from Eq. (10) in the "Methods" section) to fully capture the complexity of the ice-sheet dynamics.

Second-order effects on NGRIP thinning arise from parameterised physical processes like submarine melting, GIA, and surface ablation. The submarine melt rate primarily controls the timing and magnitude of the northeast ice front retreat triggered by the intrusion of warmer AW at the early Holocene along the NEGIS coasts[31–34,46]. A stronger ice-ocean heat flux exchange (see Eq. (7) in the "Methods" section) ensures an early onset of the northeast retreat, matching the deglaciation timings of sediment core locations from the outer and inner coast, generally inducing the ice front to retreat farther inland. However, a higher ice-ocean heat flux tends to reduce the NGRIP dropdown overall. Cooler atmospheric temperatures during the Neoglacial associated with a reduced advection of Atlantic-sourced waters promote ice regrowth towards the present ice front, causing a reduction in dynamic thinning. If such a regrowth is not outpaced by a moderate/strong active ice stream sustaining ice mass flow from the interior, such as in the case of our best simulation, surface elevation tends to increase after the HTM, reducing the total Holocene NGRIP elevation drop.

Higher lithosphere relaxation times approximating higher mantle viscosities cause a delayed bedrock response to the ice unloading during the deglaciation. A delayed bedrock uplift in the northeast, as the ice front retreats inland and ice mass is lost, keeps the bedrock elevation low enough to favour earlier sliding in streaming areas (see Eq. (3) in the "Methods" section) and leads to a prompt inland propagation of velocities. This initiates early dynamic thinning in central Greenland, causing the NGRIP surface elevation to decrease prior to the model having time to respond to the increase in snow accumulation at the Holocene onset. A northeastern higher mantle viscosity would induce an earlier thinning in north-central Greenland, extending the dropdown duration as suggested by data[2]. This would agree with the presence of a higher mantle viscosity in central Greenland[47]. Yet, a faster deformation (lower relaxation time) compares better with elevation data overall, as the model has a delayed response in the surface elevation increase around 11–10 kyr ago. A more complex GIA model accounting for lateral mantle viscosity variations would likely reduce the reconstruction-model mismatch related to such an uncertainty[48].

Enhanced surface ablation at higher latitudes (see Eq. (6) in the "Methods" section) results in higher northeast ice mass loss and grounding line retreat. The geometric reorganisation upon ice-front recession propagates velocities farther upstream, leading to a higher NGRIP elevation drop.

Mismatch between modelled-reconstructed NGRIP surface elevation change

The NGRIP thinning history simulated in our full-deglaciation simulations compares well with that estimated from ice-core data[2,4] (Figs. 2, 4a), in particular from -10 kyr ago onwards. Although the model simulates the surface elevation change through the Holocene qualitatively well, it fails to capture the full NGRIP lowering both in terms of magnitude and timing.

The residual data-model mismatch in the early Holocene could stem from the underestimated precipitation due to atmospheric warming. A comparison with Holocene NGRIP accumulation data[49,50] indicates an underestimation by -0.08 m/yr (Fig. S14a), largely attributable to the Regional Climate Model's climatological mean[51]. A supplementary test, by adjusting the reference precipitation for the 0.08 m/yr deviation in north-central Greenland, with an unvaried precipitation rate of change, shows minor improvement (-20 m) (Fig. S14). Still the response time of the NGRIP surface elevation to changes in accumulation at the early Holocene might have been faster than modelled. In fact, the rapid NGRIP elevation increase suggested by data occurs only -1 kyr after the abrupt increase in accumulation (from 11.7 to 10.7 kyr ago, Figs. 2a, f and S14). Climatic reconstructions[50] would support a faster early Holocene accumulation rise than the reanalysis precipitation signal used here[25]. A higher rate of change in accumulation could yield a faster elevation increase, possibly reducing the data-model temporal offset before 10 kyr ago.

Elevated basal ice temperatures due to higher GHF (Fig. S9) might hinder elevation gain at the early deglaciation by fostering sliding. Increased GHF aligns with borehole data indicating a temperate bed beneath NGRIP[52]. However, consensus is lacking on north-central Greenland's basal thermal state[20]. The early-Holocene elevation rise could also be affected by uncertainties in post-glacial isostatic rebound. Our approach attributes bedrock uplift solely to GrIS mass loss, neglecting the GIA signal from Innuitian ice sheet deglaciation[3], which could impact the isostatic rebound in central Greenland. Our simulations underestimate bedrock uplift in north-central Greenland by half (see Fig. S15 and Fig. 11 from ref. 5). As the North American ice-sheet system disappeared almost completely 8 kyr ago[5], including such a GIA signal might initiate an earlier NGRIP bedrock uplift, increasing the modelled surface elevation.

We attribute the temporal offset in the NGRIP lowering mainly to a simulated delay in dynamic thinning following margin retreat. The elevation decrease results from dynamic thinning outpacing the accumulation increase. In our simulations this occurs around 9.8 kyr

ago, ~800 years after the onset of the reconstructed surface elevation decrease[2]. We attribute this discrepancy to a simulated delay in the early Holocene retreat along the inner northeast coast (Fig. 3, right panel). Although the retreat from the outer-middle shelf (before 11 kyr ago) is well simulated, retreat near the present-day ice front lags by centuries (millennia for Lambert Land and Sondre Mellemland). This implies that the impact of the northeast ice stream in north-central Greenland may have occurred earlier than our simulations indicate, thereby outpacing accumulation-driven elevation rise. Furthermore, the effect of the dynamic propagation from margin retreat strongly depends on the location where the paleo-ice stream initiates. It is possible that the streaming area was situated closer to the ice divide already 10 kyr ago than shown in Fig. 1. In our model, the ice stream onset is governed by the inland extent of regions of low effective pressure (Eq. (4)). The predefined NEGIS basal friction coefficient, altered temporally (Fig. S1, left panel), dictates the potential presence of an ice stream. However, actual stream activation occurs when effective pressure dips low enough to reduce basal friction and initiate fast flow, i.e., when basal water increases due to enhanced frictional heating (Fig. S4). In our simulations, this occurred around 10 kyr ago, as the northeast ice front still retreats from the inner shelf (Fig. 1), and the increase in basal shear stress produces basal water to lubricate the bed (Fig. S4). However, the presence of an active hydrological drainage system at the NEGIS already at the early deglaciation (~11 kyr ago), and its reorganisation associated with dynamic thinning, could have induced an earlier and far-reaching paleo ice stream onset. This cannot be accurately simulated by our model as the latter takes into account only local changes in the water system[53]. In support of an earlier paleo-stream activation, Franke et al. (2022)[7] suggested that ice-stream initiation occurs likely at the beginning of the deglaciation, possibly driven by large geometry shifts, subglacial water routing variations[22], and catchment piracy[17]. An early Holocene paleo ice stream extending well inland might have induced early ice advection from north-central Greenland, decreasing the NGRIP surface elevation earlier. Finally, we cannot rule out that the retreat of the northwest coast had a non-negligible impact on the NGRIP elevation dropdown. In fact, although basal friction in northwest Greenland does not correlate well with the NGRIP thinning rate in our model (Fig. S7), it also inadequately represents northwest dynamics and retreat. We likely simulate a delayed retreat in northwest Greenland, as the applied temperature anomaly exhibits a damped early Holocene increase compared to reconstructions, which, on the contrary, indicate a rapid temperature rise before 10.5 kyr ago[3]. The early regional retreat might have initiated a stronger early Holocene dynamic thinning in the northwest, possibly affecting north-central Greenland's elevation history. Moreover, we overlook the buttressing effect of the demise of the Innuitian Ice sheet, potentially amplifying retreat from the American continent. Simulating an active ice body in Ellesmere Island connected to Greenland, inducing an earlier northwest coast retreat via stronger, earlier temperature increase at the early Holocene, might reduce this time discrepancy.

Uncertainties in the reconstructed Holocene thinning curves[2] might be underestimated, as (1) they have been estimated by assuming a homogeneous climate across Greenland[4] and (2) the uplift-corrected $\delta^{18}O$ signal used to infer the site's elevation changes does not consider the non-negligible influence of ice-load changes in the Innuitian ice sheet at the Holocene onset[3]. Such uncertainties might partly compensate for the missing elevation drop simulated at the early-Holocene.

For the period 8–0 kyr, our modelled evolution fits well within the reconstruction uncertainties. Yet, ice-core data show a greater elevation decrease throughout the last phase of the Holocene (e.g. the last ~4 kyr). Although we impose a decreased basal friction coefficient at the present NEGIS for the last simulated 8 kyr, we fail to reproduce the rate of the late-Holocene lowering. We attribute this discrepancy to the

northeast ice front advance after the HTM, which slows down the ice flow in the northeast, reducing ice advection and the NGRIP elevation decrease. Still, our late-Holocene NGRIP elevation change is consistent with previous modelling efforts evaluated against RSL estimates[4,5].

Here, we attribute at least half of the estimated NGRIP elevation drop to the dynamic thinning associated with the Northeast retreat as induced by the Holocene warming. Such dynamic thinning is the result of ice-flow acceleration in the northeast triggered by the formation and inland development of the paleo-NEGIS during the last deglaciation. Our results imply that a future northeast ice front retreat stemming from increasing temperatures might similarly provoke tens of metres of dynamic thinning in central Greenland. Given that the present-day NEGIS velocity pattern is not captured by most ice-sheet models[54], our results suggest that inland dynamic thinning in north-central Greenland is underestimated by future projections and Greenland's contribution to future sea-level rise may be greater than currently anticipated.

Methods

Ice-sheet-shelf model

We use the open-source state-of-the-art Yelmo ice-sheet model[11,55] version 1.801 (https://github.com/palma-ice/yelmo/). Yelmo is a three-dimensional, thermodynamically coupled, higher-order ice-sheet-shelf model that is here run over the Greenland domain at 8 km resolution. The model has been recently improved to adopt the depth-integrated-viscosity approximation (DIVA) velocity scheme[56,57], a higher-order stress approximation proven to be efficient for multi-millennial simulations. This solver is found to replicate well the flow found in the ice-sheet interior but also that of fast ice streams and of floating ice shelves[57].

The basal shear stress ($\boldsymbol{\tau}_b$) is defined through the regularised Coulomb friction law[58] as:

$$\boldsymbol{\tau}_b = -\beta \mathbf{u}_b = -C_b \left(\frac{|\mathbf{u}_b|}{|\mathbf{u}_b| + u_0} \right)^q \frac{\mathbf{u}_b}{|\mathbf{u}_b|}, \tag{1}$$

where $\mathbf{u}_b$ is the basal velocity, q is the exponent of the friction law and u_0 is a reference velocity parameter (100 m/yr). The bed-dependent term C_b is defined as

$$C_b = \lambda \, c_f N_{\text{eff}} \tag{2}$$

where c_f is a unitless coefficient representing the local bed characteristics. The bed-dependent term is decreased through a factor λ depending exponentially on the bedrock elevation (z_b)[55], as

$$\lambda = \begin{cases} 1 & \text{if } z_b > z_1 \\ \max \left[\exp \left(\frac{z_b - z_1}{z_1 - z_0} \right), \lambda_{\min} \right] & \text{if } z_b < z_1 \end{cases} \tag{3}$$

with $z_1 = 400$ m and z_0 as a tunable parameter. This relationship ensures that ice flows faster in topographic depressions[55]. The parameter c_f is set to a constant value everywhere, except in the northeastern basin. Here, c_f is reduced to better capture the system of paleo and present ice-streams (Fig. S1). In this way, we attempt to replicate the recent findings from radio stratigraphy analysis suggesting that at least part of the Holocene was characterised by the presence of a NEGIS-like stream located to the north of the present NEGIS and now deactivated[7]. We outline this paleo NEGIS following the location of the internal deformation features (folds) found from radargrams. This allows us to define a stream that extends along the northern part of the northeast catchment from the 79°N glacier towards the ice divide (northern branch of Fig. S1). The present NEGIS (southern and central branches) has been set as a region characterised by present surface velocities >30 m/yr for latitudes < 77.5°N and by velocities > 50 m/yr

for higher latitudes. This approach defines a long penetrating stream in correspondence with the present-day main branch and a more constrained streaming region in the upper tail. The central branch of the ice stream is kept active for the whole simulation with a fixed value (f_{mid}). There is great uncertainty around the timing of activation/ deactivation of this ice-stream system and the processes that might have caused it. Yet, significant restructuring of the ice stream's shape and strength is more probable during the initial phase of deglaciation due to the large ice-sheet geometrical reorganisations upon margin retreat. Therefore we assume an abrupt relocation of the ice-stream flow from its past to its present position around 8 kyr ago. This is also supported by the recent hypothesis of the NEGIS showing a similar configuration to today since 8000 years ago[16]. To this end, c_f is linearly reduced in the southern branch to f_{min} to favour the build-up of faster flow along the present-day NEGIS, even as the ice sheet re-advances during the Neoglacial. This ensures a further reduction of the NGRIP surface elevation (Fig. S13). Therefore, in our simulations, c_f can be set to either 1, or f_{mid} or f_{min} depending on the considered NEGIS branch and time in the Holocene (Fig. S1). The parameters f_{mid} and f_{min} are perturbed in our simulations (see Table S1). Although our approach approximates the past activation/deactivation of the northeast ice stream through an imposed relocation of the paleo ice stream to its present position, the root causes of such an internal switch are not investigated. The timing and the form set for the internal switch between the ice-stream modes have negligible effects on the NGRIP surface elevation lowering (Fig. S16). We investigate a potential effect also for different ice-stream configurations and we conclude that considering both streams active at the same time instead of an abrupt switch during the Holocene has a marginal impact on our results (Fig. S16). Also, it should be noted that in our simulations, the presence of an active northern branch for part of the Holocene is not crucial for triggering the NGRIP dropdown. On the contrary, the activation of the elongated ice stream in the southern branch at 8 kyr ago, propagating several hundreds of km inland (Fig. 1), ensures a sustained dynamic adjustment in north-central Greenland driving the NGRIP dropdown (Fig. S5, lower panel). Conversely, an unperturbed simulation restricts the inland velocity propagation to lower elevations (Fig. S11), limiting the effect of the stream activity at the NGRIP site (Fig. S13). The c_f term reduced at the NEGIS (f_{mid}) is the dominant term within the basal friction parameters to directly influence the NGRIP thinning rate at the early-mid Holocene, as suggested by the high correlation between the two (Fig. S8).

The effective pressure N_{eff} is computed through the relationship for till hydrology[53], such that

$$N_{eff} = N_0 \left(\frac{\delta P_0}{N_0}\right)^s 10^{\left(\frac{e_0}{C_c}\right)(1-s)} \tag{4}$$

where $P_0 = \rho_i g H$ and $s = \frac{W_{til}}{W_{til}^{max}}$ is the fraction of basal water in till (W_{til}) over its maximum value held by the saturated till (W_{til}^{max} here set to 2 m). Values of e_0 and C_c are set as in ref. 53, whilst the fraction (δ) of the overburden pressure P_0 is considered here as a tunable parameter. W_{til} evolves in Yelmo as

$$\frac{\partial W_{til}}{\partial t} = -\frac{\rho}{\rho_w}\dot{b}_g - C_d \tag{5}$$

where the basal mass balance, $\dot{b}_g$, is computed for grounded regions. Such a subglacial hydrological scheme only accounts for local changes in the water system and the till rate of drainage C_d is fixed and set to 0.001 m/yr.

The surface ablation is calculated by the insolation-temperature melt (ITM[59]) method, a simplified scheme that, contrary to PDD schemes, directly accounts for insolation changes and melt changes

due to surface albedo. The potential surface melt is calculated as

$$M_s = \frac{\Delta t}{\rho_w L_m} \left[\tau_a(1-\alpha_s)S + c + \lambda T\right] \tag{6}$$

where $c = c_1 + b \,(\text{lat}-\text{lat}_0)$, L_m is the latent heat of melting, α_s is the surface ice or snow albedo, S is the incoming insolation, Δt is the day length and λ is the long-wave radiation coefficient (10 W/m² K). The terms b and c_1 correct the surface ablation for high-latitude regions and the ice sheet uniformly, respectively. τ_a is the atmosphere transmissivity, calculated as $\tau_a = 0.46 + 0.00006(z_s)^{0.5}$, where z_s is the surface elevation[60]. The reference latitude lat_0 is set to 65°N and both b and c_1 are considered as tunable parameters.

A flow enhancement factor is introduced in Glen's flow law to approximate the effect of ice anisotropy on the ice flow[11]. Specific flow factors depending on the flow regime can be assigned in the model. The enhancement factor for floating areas (E_{shelf}) is set equal to 0.7, that for streaming zones (E_{stream}) is set to 1, whilst that for shearing-driven regions (E_{shear}) is considered as a tunable parameter. Subsequently, the shear and stream enhancement factors are averaged for grounded areas, with the weighting determined by the vertical shearing fraction computed at every grid cell[11].

Bedrock elevation changes are computed via the Elastic Lithosphere Relaxing Asthenosphere (ELRA) scheme[61]. This simple but effective glacial isostatic adjustment (GIA) scheme assumes viscoelastic deformation of the crust from the elastic behaviour of the lithosphere and the ability of the asthenosphere to relax upon ice load changes. Here the rigidity of the lithosphere (H_e, see Fig. S8) and the upper mantle relaxation time (τ, see Fig. S8) are considered perturbation parameters in our ensemble.

The calving rate is calculated following the Von Mises stress criterion[62], here rewritten in terms of strain rates[56]. The constant value κ_t from Eq. (73) of ref. 56 is here interpreted as a tunable parameter. The submarine melting around the ice sheet is computed through the anomaly method described in[63], such that

$$B_m(t) = B_{ref} + \kappa \,\Delta T_{ocn}(t) \tag{7}$$

where B_{ref} is a reference melting rate (set as equal to 1 m/yr) and ΔT_{ocn} is the paleoclimatic ocean temperature anomaly around Greenland. κ is the ice-water heat flux coefficient (also called sensitivity factor), and it is treated as a tunable parameter. Melt below the ice shelves is considered here as the 10% of the grounding line melt.

Climate and ocean forcings

In the main experiment, the model is forced with a full-deglaciation climatology at a high temporal resolution over Greenland, similar to ref. 30. Atmospheric temperature is defined as

$$T_{atm}(t) = T_{ref} + \Delta T_{atm}(t) \tag{8}$$

where ΔT_{atm} is the 22kyr-long monthly temperature anomaly from the fully coupled atmosphere-ocean TraCE-21ka experiment corrected for the AMOC strength[24]. Precipitation changes over the Holocene are imposed as

$$P(t) = P_{ref} \cdot P_f(t) \tag{9}$$

where the past precipitation fraction P_f is calculated at sea level through this precipitation–temperature relationship:

$$P_f(t) = P(t) \cdot \exp(-f_p \cdot (T_{atm} - T_{sealevel})). \tag{10}$$

$T_{sealevel}$ is the atmospheric temperature corrected at sea level, as $T_{atm} + \delta_z \cdot \gamma_{atm}$, where γ_{atm} is the atmospheric lapse rate and δ_z is the

climatology-modelled surface elevation anomaly. $P(t)$ is the 20-kyr spatially variable precipitation fraction reanalysis reconstructed from a new ice-core data assimilation approach[25], and f_p is the precipitation scaling factor for past temperature anomalies (similar to β of Eq. (8) of ref. 25). This factor should be defined as spatially variable to represent the heterogeneous precipitation-temperature relationship throughout the ice sheet[25], however, we consider it as a tunable parameter only for the Northeast basin. Three different precipitation scenarios $P(t)$ (low, moderate, high) representing the relative amount of accumulation during the deglaciation are generated. Here, we use the high precipitation scenario, which suggests a rapid and substantial increase in accumulation in the early Holocene. P_{ref} has been processed to refer to the 1981–2010 climatology of ref. 51 as T_{ref}.

Transient ocean temperature anomalies ΔT_{ocn} are taken from the TraCE-21ka main experiment[26]. Temperatures are averaged at 300–350 m in the ocean column. We correct the TraCE-21ka temperature anomaly for the Northeast marine basin with a homogeneous temperature signal that mimics the continuous advection of subsurface warmer Atlantic Water (AW) to the shelf from the early to the mid-Holocene, following the well-constrained evidence from sediment core analysis ([33] and references therein). The corrected signal shows a positive subsurface ocean temperature anomaly with respect to glacial conditions already at 13.3 kyr BP, a time that represents the minimum age of presence of AW found in both troughs in the northeast[31,32]. ΔT_{ocn} is set as constant until 10 kyr BP, after which it declines slowly until 7.5 kyr BP. A subsequent cooldown of subsurface waters due to the reduced intrusion of AW in the shelf[31–34] is then approximated by a constant low-temperature anomaly until almost the end of the Holocene (the oceanic temperature anomaly recovers to present values during the last 100 years, see Fig. S3). In this setup, maximum and minimum Holocene-present temperature anomalies are defined as +2 °C (early Holocene) and −1 °C (mid-late Holocene). The anomaly from the late glacial to the early Holocene corresponds well with the warming of ~3 K found from marine records of subsurface ocean temperature in Farm Strait[64].

In an additional explorative test, the model is forced by one of the Greenland-wide 20 kyr-to-present annual air temperature scenarios reconstructed through the paleoclimatic assimilation technique presented in ref. 25 (S3 scenario). Here, annual temperature anomalies are converted into monthly fields by applying the seasonal variability from temperature data from ref. 24, having them smoothed below 50 yr through a low-pass Butterworth filter. The considered scenario has been reconstructed by assuming a spatially homogeneous but stronger precipitation seasonality. We choose this scenario among the others available because (1) it is one of only two scenarios that, by applying a monthly anomaly, allows a proper glacial expansion, and (2) it presents the sharpest early-Holocene transition, approximating best the temperature signal of ref. 24. Here, precipitation and oceanic temperatures are the same as in the main experiment.

Deglaciation simulations

A classic steady-state spin-up approach is used for model initialisation. The ice sheet is allowed to freely evolve under LGM (~20 kyr ago) conditions for 50 kyr to reach the thermomechanical equilibrium[54]. The model is then forced toward the present by the transient climatologies described above. Full deglaciation experiments are performed for a large ensemble of 3000 simulations where five basal friction parameters ($f_{mid}, f_{min}, q, z_0, \delta$), three climate variables (c_1, b and f_p), two isostasy-related parameters (H_e and τ), two frontal/submarine ablation terms (κ_t and κ) and one material property (E_{shear}) are perturbed using the Latin Hypercube Sampling approach (e.g., ref. 59) (see Table S1 for an overview of the perturbed parameters). Note that while q, z_0, δ, c_1 and b are set as uniform around Greenland, the friction coefficient parameter is changed only beneath the northern/southern/centre branches of the NEGIS, following the temporal scheme of Fig. S1. All other basins hold the same $c_f = 1$. This approach allows us to

directly evaluate the effect of a fast-flowing ice stream on the thinning in central Greenland. The ice-sheet topography is taken from Bed-Machine v3[62]. The bedrock elevation is reduced by 1−σ beneath the main tail of both paleo and present NEGIS to constrain the direction of the flow during the retreat, where σ is the BedMachine-estimated elevation uncertainty (Fig. S17, left panel). This simple approach allows us to reproduce both the northern paleo NEGIS-like ice stream that was active during the Holocene and the complex present-day NEGIS velocity pattern after a full deglaciation simulation with unprecedented detail (Fig. 1). The geothermal heat flow is prescribed as in ref. 12 below the ice sheet and as in ref. 65 outside the continental borders.

Validation process

The large ensemble undergoes a validation test to rank the goodness of the model simulations and to statistically weigh the results. The approach follows a simple averaging skill-score method based on a Gaussian error distribution[66]. For each ensemble member, we calculate 13 individual scores based on paleo and present model-data misfits and then aggregate them into a single total score. However, contrary to ref. 66, here we do not account for data and structure model uncertainties in the misfit calculation. The misfits considered are: mean-square error (MSE) of modelled to observed present GrIS thickness (H_{PD}, data from ref. 62), MSE of modelled to observed present GrIS surface velocity (U_{PD}, data from ref. 67), absolute modelled-observed modern surface elevation difference at NGRIP ($S_{NGRIP_{PD}}$, data from ref. 68), MSE of modelled to reconstructed deglaciation elevation changes at NGRIP ($S_{NGRIP_{DG}}$, data from ref. 2), MSE of modelled to observed present GrIS ice-covered area (A_{PD}, data from ref. 62) and MSE of modelled to observed ice-covered area at the LGM (A_{LGM}, data from ref. 5). The errors H_{PD}, U_{PD} and A_{PD} are additionally calculated for the northeast sector only, so that three further misfits are considered (H_{NE}, U_{NE}, and A_{NE}). Moreover, we calculate the MSE of modelled-observed deglaciation timings computed and averaged (1) at four sediment core locations from the northeast continental shelf ($T_{SED_{DG}}$, data from refs. 31–34), 2) at three locations in the outer shelf as calculated from ^{10}Be exposures dates from morain/boulder samples ($T_{OUT_{DG}}$, data from ref. 14) and (3) at other six locations closer to the present NEGIS ice front ($T_{IN_{DG}}$, data from ref. 14) (see Fig. 3). For moraine and boulder data, deglaciation occurs when the cell is modelled as partially or completely ice-free. For sediment core data, we consider a point as deglaciated if it is either ice-free or still presents a floating shelf, as the paleoenvironment interpretation of such data is uncertain. Errors in the deglaciation timing are here calculated with respect to the time interval of 10.2–9.6 kyr ago for ref. 34, 13.4–11.2 kyr ago for ref. 31, 10.9–10 kyr ago for ref. 33 and 14.0–13.3 kyr ago for ref. 32. The resulting three marine-moraine MSEs describe the lag in simulating the time of deglaciation of specific locations in the northeast sector during the early Holocene. Finally, we introduce a last binary control on the upstream retreat of 79°N glacier: simulations that retreated more than 70 km upstream will present a maximum error.

Each misfit $M_{i,j}$, where i is the data class and j is the ensemble simulation, is then interpreted as a score $S_{i,j}$ following the equation[66]:

$$S_{i,j} = \exp(-M_{i,j}/\text{median}(M_{i,j})). \tag{11}$$

The simple multiplication of the 13 S_{ij} yields the simulation-dependent total score S_j:

$$S_j = \prod_{i=1} S_{i,j} \tag{12}$$

which is further normalised between 1 (best simulation) and 0 (worst simulation). We assume a good total score if it is higher than the product of the mean score for each misfit for best simulations, i.e. $1e^{-7}$ (Fig. S10). Thus, the score-weighted ensemble mean of a variable x is

calculated as

$$\overline{x} = \frac{\sum_{j=1} x_j \cdot S_j}{\sum_{j=1} S_j} \qquad (13)$$

with its standard deviation as

$$\sigma_x = \sqrt{\frac{\sum_{j=1}(x_j - \overline{x})^2 \cdot S_j}{\frac{N-1}{N}\sum_{j=1} S_j}} \qquad (14)$$

where N is the total number of ensemble members.

To further reduce the uncertainty in our model results, we add another constraint that distinctly separates plausible from implausible model representations within the ensemble. Following this approach, simulations are considered valid as long as the absolute elevation difference between modelled and observed elevations is <50 m (e.g., $S_{NGRIP_{PD}}$ <50 m) so that 563 simulations over 3000 are retained as valid. This additional constraint rewards simulations exhibiting an accurate fit to present-day elevation data, whose errors in the estimate are usually below 10 m. Thus, the ensemble statistics are calculated only for this subset of valid simulations. This means that we calculate the score-weighted mean and standard deviation of the plausible simulations only within the ensemble ($N = 563$). All simulations are a priori considered equally likely (i.e., given equal weight in the statistics).

Data availability

Transient climatologies from Buizert et al. (2018)[24] and Badgeley et al. (2020)[25] are available at https://www.ncdc.noaa.gov/paleo-search/study/23430 and https://doi.org/10.18739/A2599Z26M, respectively. Reference climate from Box (2013)[51] is found at https://zenodo.org/record/3359192#.YUmIiHvRYYs. TraCE-21ka simulations are available at https://www.earthsystemgrid.org/project/trace.html. The best model simulation generated in this study has been deposited in the ZENODO database at https://doi.org/10.5281/zenodo.12667358. All other Yelmo simulations presented here are available upon request.

Code availability

The Yelmo ice-sheet model can be freely downloaded from https://github.com/palma-ice/yelmo/. The modules used to compute all boundary conditions for the Greenland Ice Sheet are stored in https://github.com/palma-ice/yelmox (here version 1.801, tag "ngrip-thinning" is used). R scripts used for the ensemble analysis are available at https://github.com/ilaria-tab/ngrip_thinning.git.

References
1. Fischer, H. et al. Palaeoclimate constraints on the impact of 2C anthropogenic warming and beyond. *Nat. Geosci.* **11**, 474–485 (2018).
2. Vinther, B. et al. Holocene thinning of the Greenland ice sheet. *Nature* **461**, 385–388 (2009).
3. Lecavalier, B. S. et al. High Arctic Holocene temperature record from the Agassiz ice cap and Greenland ice sheet evolution. *Proc. Natl Acad. Sci. USA* **114**, 5952–5957 (2017).
4. Lecavalier, B. S. et al. Revised estimates of Greenland ice sheet thinning histories based on ice-core records. *Quat. Sci. Rev.* **63**, 73–82 (2013).
5. Lecavalier, B. S. et al. A model of Greenland ice sheet deglaciation constrained by observations of relative sea level and ice extent. *Quat. Sci. Rev.* **102**, 54–84 (2014).
6. Rignot, E. & Mouginot, J. Ice flow in Greenland for the international polar year 2008–2009. *Geophys. Res. Lett.* **39**, 11 (2012).
7. Franke, S. et al. Holocene ice-stream shutdown and drainage basin reconfiguration in northeast Greenland. *Nat. Geosci.* **15**, 995–1001 (2022).
8. Rückamp, M., Greve, R. & Humbert, A. Comparative simulations of the evolution of the Greenland ice sheet under simplified Paris Agreement scenarios with the models SICOPOLIS and ISSM. *Polar Sci.* **21**, 14–25 (2019).
9. Beyer, S., Kleiner, T., Aizinger, V., Rückamp, M. & Humbert, A. A confined–unconfined aquifer model for subglacial hydrology and its application to the Northeast Greenland Ice Stream. *Cryosphere* **12**, 3931–3947 (2018).
10. Smith-Johnsen, S., de Fleurian, B., Schlegel, N., Seroussi, H. & Nisancioglu, K. Exceptionally high heat flux needed to sustain the Northeast Greenland Ice Stream. *Cryosphere* **14**, 841–854 (2020).
11. Robinson, A. et al. Description and validation of the ice-sheet model Yelmo (version 1.0). *Geosci. Model Dev.* **13**, 2805–2823 (2020).
12. Martos, Y. M. et al. Geothermal heat flux reveals the Iceland hotspot track underneath Greenland. *Geophys. Res. Lett.* **45**, 8214–8222 (2018).
13. Arndt, J. E., Jokat, W. & Dorschel, B. The last glaciation and deglaciation of the Northeast Greenland continental shelf revealed by hydro-acoustic data. *Quat. Sci. Rev.* **160**, 45–56 (2017).
14. Larsen, N. K. et al. Instability of the Northeast Greenland Ice Stream over the last 45,000 years. *Nat. Commun.* **9**, 1872 (2018).
15. Bennike, O. & Weidick, A. Late Quaternary history around Nioghalvfjerdsfjorden and Jøkelbugten, North-East Greenland. *Boreas* **30**, 205–227 (2001).
16. Gerber, T. A. et al. Upstream flow effects revealed in the EastGRIP ice core using Monte Carlo inversion of a two-dimensional ice-flow model. *Cryosphere* **15**, 3655–3679 (2021).
17. Brouard, E. & Lajeunesse, P. Ice-stream flow switching by up-ice propagation of instabilities along glacial marginal troughs. *Cryosphere* **13**, 981–996 (2019).
18. Benediktsson, Í. Ö., Aradóttir, N., Ingólfsson, Ó. & Brynjólfsson, S. Cross-cutting palaeo-ice streams in NE-Iceland reveal shifting Iceland Ice Sheet dynamics. *Geomorphology* **396**, 108009 (2022).
19. Rogozhina, I. et al. Melting at the base of the Greenland ice sheet explained by Iceland hotspot history. *Nat. Geosci.* **9**, 366–369 (2016).
20. MacGregor, J. A. et al. A synthesis of the basal thermal state of the Greenland Ice Sheet. *J. Geophys. Res.: Earth Surf.* **121**, 1328–1350 (2016).
21. Karlsson, N. B. et al. A first constraint on basal melt-water production of the Greenland ice sheet. *Nat. Commun.* **12**, 3461 (2021).
22. Karlsson, N. B. & Dahl-Jensen, D. Response of the large-scale subglacial drainage system of Northeast Greenland to surface elevation changes. *Cryosphere* **9**, 1465–1479 (2015).
23. Grinsted, A. et al. Accelerating ice flow at the onset of the Northeast Greenland Ice Stream. *Nat. Commun.* **13**, 5589 (2022).
24. Buizert, C. et al. Greenland-wide seasonal temperatures during the last deglaciation. *Geophys. Res. Lett.* **45**, 1905–1914 (2018).
25. Badgeley, J. A., Steig, E. J., Hakim, G. J. & Fudge, T. J. Greenland temperature and precipitation over the last 20 000 years using data assimilation. *Climate* **16**, 1325–1346 (2020).
26. Liu, Z. et al. Transient simulation of last deglaciation with a new mechanism for Bølling–Allerød warming. *Science* **325**, 310–314 (2009).
27. Cartapanis, O., Jonkers, L., Moffa-Sanchez, P., Jaccard, S. L. & de Vernal, A. Complex spatio-temporal structure of the Holocene Thermal Maximum. *Nat. Commun.* **13**, 5662 (2022).
28. Westhoff, J. et al. Melt in the Greenland EastGRIP ice core reveals Holocene warm events. *Climate* **18**, 1011–1034 (2022).
29. Axford, Y., De Vernal, A. & Osterberg, E. C. Past warmth and its impacts during the Holocene thermal maximum in Greenland. *Annu. Rev. Earth Planet. Sci.* **49**, 279–307 (2021).
30. Briner, J. P. et al. Rate of mass loss from the Greenland Ice Sheet will exceed Holocene values this century. *Nature* **586**, 70–74 (2020).

31. Davies, J. et al. Linkages between ocean circulation and the Northeast Greenland Ice Stream in the Early Holocene. *Quat. Sci. Rev.* **286**, 107530 (2022).

32. Hansen, K. E. et al. Deglacial to Mid Holocene environmental conditions on the northeastern Greenland shelf, western Fram Strait. *Quat. Sci. Rev.* **293**, 107704 (2022).

33. Lloyd, J. et al. Ice-ocean interactions at the Northeast Greenland Ice stream (NEGIS) over the past 11,000 years. *Quat. Sci. Rev.* **308**, 108068 (2023).

34. Syring, N. et al. Holocene interactions between glacier retreat, sea ice formation, and Atlantic water advection at the inner Northeast Greenland continental shelf. *Paleoceanogr. Paleoclimatol.* **35**, e2020PA004019 (2020).

35. An, L. et al. Ocean melting of the Zachariae Isstrøm and Nioghalvfjerdsfjorden glaciers, northeast Greenland. *Proc. Natl Acad. Sci. USA* **118**, e2015483118 (2021).

36. Khan, S. A. et al. Sustained mass loss of the northeast Greenland ice sheet triggered by regional warming. *Nat. Clim. Change* **4**, 292–299 (2014).

37. Choi, Y., Morlighem, M., Rignot, E., Mouginot, J. & Wood, M. Modeling the response of Nioghalvfjerdsfjorden and Zachariae Isstrøm glaciers, Greenland, to ocean forcing over the next century. *Geophys. Res. Lett.* **44**, 11–071 (2017).

38. Schaffer, J. et al. Bathymetry constrains ocean heat supply to Greenland's largest glacier tongue. *Nat. Geosci.* **13**, 227–231 (2020).

39. Bentley, M. J. et al. Direct measurement of warm Atlantic Intermediate Water close to the grounding line of Nioghalvfjerdsfjorden (79˚N) Glacier, northeast Greenland. *Cryosphere* **17**, 1821–1837 (2023).

40. Williams, C. R., Hindmarsh, R. C. & Arthern, R. J. Frequency response of ice stream. *Proc. R. Soc. A* **468**, 3285–3310 (2012).

41. Wang, W., Li, J. & Zwally, H. J. Dynamic inland propagation of thinning due to ice loss at the margins of the Greenland ice sheet. *J. Glaciol.* **58**, 734–740 (2012).

42. Khan, S. A. et al. Extensive inland thinning and speed-up of Northeast Greenland Ice Stream. *Nature* **611**, 727–732 (2022).

43. Williams, J. J., Gourmelen, N. & Nienow, P. Complex multi-decadal ice dynamical change inland of marine-terminating glaciers on the Greenland Ice Sheet. *J. Glaciol.* **67**, 833–846 (2021).

44. Reese, R., Gudmundsson, G. H., Levermann, A. & Winkelmann, R. The far reach of ice-shelf thinning in Antarctica. *Nat. Clim. Change* **8**, 53–57 (2018).

45. Gerber, T. A. et al. Crystal orientation fabric anisotropy causes directional hardening of the Northeast Greenland Ice Stream. *Nat Commun* **14**, 2653 (2023).

46. Smith, J. A. et al. Holocene history of the 79°N ice shelf reconstructed from epishelf lake and uplifted glaciomarine sediments. *Cryosphere* **17**, 1247–1270 (2023).

47. Kappelsberger, M. T. et al. Modeled and observed bedrock displacements in north-east Greenland using refined estimates of present-day ice-mass changes and densified GNSS measurements. *J. Geophys. Res.: Earth Surf.* **126**, e2020JF005860 (2021).

48. Coulon, V. et al. Contrasting response of West and East Antarctic ice sheets to glacial isostatic adjustment. *J. Geophys. Res.: Earth Surf.* **126**, e2020JF006003 (2021).

49. Gkinis, V., Simonsen, S. B., Buchardt, S. L., White, J. & Vinther, B. M. Water isotope diffusion rates from the NorthGRIP ice core for the last 16,000 years—glaciological and paleoclimatic implications. *Earth Planet. Sci. Lett.* **405**, 132–141 (2014).

50. Kindler, P. et al. Temperature reconstruction from 10 to 120 kyr b2k from the NGRIP ice core. *Climate* **10**, 887–902 (2014).

51. Box, J. E. Greenland ice sheet mass balance reconstruction. Part II: Surface mass balance (1840–2010). *J. Clim.* **26**, 6974–6989 (2013).

52. Dahl-Jensen, D., Gundestrup, N., Gogineni, S. P. & Miller, H. Basal melt at NorthGRIP modeled from borehole, ice-core and radio-echo sounder observations. *Ann. Glaciol.* **37**, 207–212 (2003).

53. Bueler, E. & van Pelt, W. Mass-conserving subglacial hydrology in the Parallel Ice Sheet Model version 0.6. *Geosci. Model Dev.* **8**, 1613–1635 (2015).

54. Goelzer, H. et al. Design and results of the ice sheet model initialisation experiments initMIP-Greenland: an ISMIP6 intercomparison. *Cryosphere* **12**, 1433–1460 (2018).

55. Blasco, J., Alvarez-Solas, J., Robinson, A. & Montoya, M. Exploring the impact of atmospheric forcing and basal drag on the Antarctic Ice Sheet under Last Glacial Maximum conditions. *Cryosphere* **15**, 215–231 (2021).

56. Lipscomb, W. H. et al. Description and evaluation of the community ice sheet model (CISM) v2. 1. *Geosci. Model Dev.* **12**, 387–424 (2019).

57. Robinson, A., Goldberg, D. & Lipscomb, W. H. A comparison of the stability and performance of depth-integrated ice-dynamics solvers. *Cryosphere* **16**, 689–709 (2022).

58. Joughin, I., Smith, B. E. & Schoof, C. G. Regularized Coulomb friction laws for ice sheet sliding: application to Pine Island Glacier, Antarctica. *Geophys. Res. Lett.* **46**, 4764–4771 (2019).

59. Robinson, A., Alvarez-Solas, J., Calov, R., Ganopolski, A. & Montoya, M. MIS-11 duration key to disappearance of the Greenland ice sheet. *Nat. Commun.* **8**, 16008 (2017).

60. Robinson, A., Calov, R. & Ganopolski, A. An efficient regional energy-moisture balance model for simulation of the Greenland Ice Sheet response to climate change. *Cryosphere* **4**, 129–144 (2010).

61. Le Meur, E. & Huybrechts, P. A comparison of different ways of dealing with isostasy: examples from modelling the Antarctic ice sheet during the last glacial cycle. *Ann. Glaciol.* **23**, 309–317 (1996).

62. Morlighem, M. et al. BedMachine v3: Complete bed topography and ocean bathymetry mapping of Greenland from multibeam echo sounding combined with mass conservation. *Geophys. Res. Lett.* **44**, 11–051 (2017).

63. Tabone, I., Robinson, A., Alvarez-Solas, J. & Montoya, M. Submarine melt as a potential trigger of the North East Greenland Ice Stream margin retreat during Marine Isotope Stage 3. *Cryosphere* **13**, 1911–1923 (2019).

64. Werner, K. et al. Holocene sea subsurface and surface water masses in the Fram Strait—comparisons of temperature and sea-ice reconstructions. *Quat. Sci. Rev.* **147**, 194–209 (2016).

65. Shapiro, N. M. & Ritzwoller, M. H. Inferring surface heat flux distributions guided by a global seismic model: particular application to Antarctica. *Earth Planet. Sci. Lett.* **223**, 213–224 (2004).

66. Pollard, D., Chang, W., Haran, M., Applegate, P. & DeConto, R. Large ensemble modeling of the last deglacial retreat of the West Antarctic Ice Sheet: comparison of simple and advanced statistical techniques. *Geosci. Model Dev.* **9**, 1697–1723 (2016).

67. Joughin, I., Smith, B. E. & Howat, I. Greenland Ice Mapping Project: ice flow velocity variation at sub-monthly to decadal timescales. *Cryosphere* **12**, 2211–2227 (2018).

68. North Greenland Ice Core Project members. High-resolution record of Northern Hemisphere climate extending into the last interglacial period. *Nature* **431**, 147–151 (2004).

Author contributions

I.T. carried out the model experiments and the statistical analysis and wrote the paper. I.T., A.R., M.M. and J.A.-S. contributed to conceiving the study and editing the manuscript.

Competing interests

The authors declare no competing interests.

Additional information

Supplementary information The online version contains supplementary material available at https://doi.org/10.1038/s41467-024-50772-5.

Correspondence and requests for materials should be addressed to Ilaria Tabone.

Peer review information *Nature Communications* thanks Richard Jones, Benjamin Keisling, Lev Tarasov and the other, anonymous, reviewer for their contribution to the peer review of this work. A peer review file is available.

Reprints and permissions information is available at http://www.nature.com/reprints

Publisher's note Springer Nature remains neutral with regard to jurisdictional claims in published maps and institutional affiliations.